CRYSTAL GROWTH & DESIGN

Article

Cite This: Cryst. Growth Des. 2018, 18, 1560−1570

pubs.acs.org/crystal

Nucleation and Growth Kinetics for Combined Cooling and Antisolvent Crystallization in a Mixed-Suspension, Mixed-Product Removal System: Estimating Solvent Dependency

Jennifer M. Schall, Jasdeep S. Mandur, Richard D. Braatz, and Allan S. Myerson*

Novartis-MIT Center for Continuous Manufacturing and Department of Chemical Engineering, Massachusetts Institute of Technology, 77 Massachusetts Avenue, Cambridge, Massachusetts 02139, United States

Supporting Information

ABSTRACT: Combined cooling and antisolvent crystallization is a critical unit operation in pharmaceutical manufacturing, especially for heat-sensitive or poorly soluble active pharmaceutical ingredients. The model-based design of these systems relies on the accuracy of the underlying growth and nucleation kinetic parameters. Unlike temperature where these kinetic parameters are well-known to follow an Arrhenius relation, their dependency on solvent composition still remains unclear, especially in continuous mixed-suspension, mixed-product removal (MSMPR) systems. In this paper, we use population balance modeling coupled with nonlinear regression to estimate growth and nucleation parameters as a function of both temperature and solvent composition. As solvent composition increases from 44 vol % to 66 vol % solvent, both growth and nucleation rates were observed to decrease monotonically with their values reduced by almost one-third. It was also shown that, if the solvent dependency is ignored, the yield can be overpredicted or underpredicted by as much as 15%.

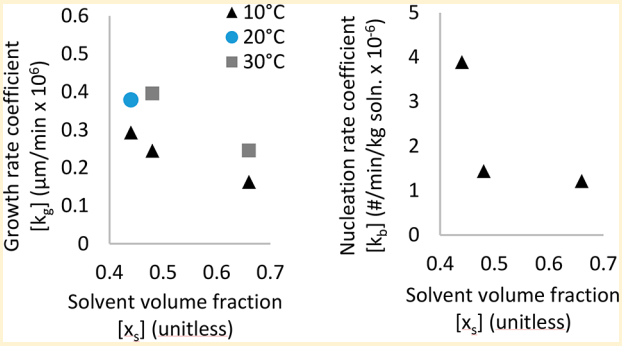

INTRODUCTION

Crystallization is the most important separation and purification method in the pharmaceutical industry, a critical unit operation in the production of more than 90% of active pharmaceutical ingredients (APIs) and 70% of solid chemicals.[1,2] The overarching goal of crystallization is to provide a consistently formulated product to customers with acceptable cost, yield, purity, and material properties.

Operating conditions in crystallizer processes can enable specifications on final product yield, purity, crystal size distribution (CSD), and morphology to be met in a single unit operation.[3] Traditionally, most industrial pharmaceutical crystallizations are batch processes. However, a shift toward continuous manufacturing is occurring to decrease costs and increase control, where process modeling is used to design and improve crystallization.[4−8] For early stage process designs, time and API availability are generally limited, so viable steady-state models that require limited experimental data are particularly useful.

A proper crystallization process model for control contains two parts: a population balance model and a kinetic model.[9] Without proper understanding of both models, the crystallization process cannot be reliably modeled and controlled. Using population balances developed by Randolph and Larson in the 1970s, researchers have been able to model and predict crystallization kinetics in a variety of continuous systems.[10,11] Cooling crystallization systems are typically modeled, as the temperature effects on crystallization are well understood.[12] However, antisolvent crystallization kinetics models are yet to be constructed using first principles. Researchers and process design engineers desire parameters based on crystallizer-independent kinetics which include solvent-composition effects and enable simulation of wide crystallizer operating ranges. Neglecting the influence of solvent composition in antisolvent crystallization systems could lead to model errors, especially in systems that are sensitive to changes in kinetic parameters.[13,14]

Multiple studies of crystal nucleation and growth kinetics in antisolvent systems exist for batch crystallization, but these studies only account for primary nucleation and/or crystal growth and exist for transient, low supersaturation ranges. In each batch study, the functional forms of model parameters for antisolvent crystallization are empirical models, based on polynomial, power law, or linear fits of regressed experimental data from batch crystallizations. Granberg and associates claimed that the degree of supersaturation has a significantly stronger influence on growth kinetics in batch crystallizations after observing that higher initial supersaturation yielded high supersaturation decay and a larger crystal growth area.[15] While publications exist that demonstrate batch crystallization processes where the composition of solvent-antisolvent mixture appears to have little to no influence on crystal nucleation and growth kinetics beyond changes in

Received: November 1, 2017
Revised: January 17, 2018
Published: January 31, 2018

DOI: 10.1021/acs.cgd.7b01528
Cryst. Growth Des. 2018, 18, 1560−1570

supersaturation, many API-solvent mixture systems cannot be acceptably modeled without accounting for these dependencies.[16−20] Nonoyama and colleagues found that using a power-law model for the solvent-composition dependence of k_g in growth kinetic models enabled the refinement of antisolvent crystallization models for an organic API in organic-aqueous antisolvent batch crystallizations.[21] Trifkovic echoed the need to model antisolvent crystallization growth parameters as functions of solvent-composition, developing a polynomial model for k_g and a linear model for g based on antisolvent mass fraction in the paracetamol/isopropanol/water batch system.[22] To thoroughly model and design a continuous crystallization process, antisolvent effects on kinetics should be considered, and the kinetic parameter regression must be updated for continuous versus batch crystallization.

Currently, researchers lack a systematic and generalized approach for mixed-suspension, mixed-product removal (MSMPR) cascade design that accounts for antisolvent effects on growth and nucleation parameters. Furthermore, procedures for regressing kinetic parameters from batch experiments tend to separate growth and nucleation events. They have limited ability to predict solvent effects on secondary nucleation kinetics, which dominates nucleation in typical MSMPR systems.[23] Kinetic parameter regression from continuous, single-stage MSMPR operation overcomes these difficulties, enabling simultaneous regression of growth and secondary nucleation kinetic parameters. To our knowledge, no previous study has demonstrated the effects of solvent composition on secondary nucleation or the effect of solvent composition on kinetic parameters in continuous antisolvent crystallizers, where substantially higher supersaturations are maintained during the crystallization process.

In this paper, we present strategies for constructing empirical growth and nucleation kinetic models to enable continuous crystallizer design and operation. First, we demonstrate that kinetic parameters, which are functions of both solvent composition and temperature, can be regressed using experimental data collected during steady-state MSMPR operation in a limited number of experiments. Next, we establish that both growth and nucleation kinetic parameters are functions of solvent composition, showing that solvent effects on nucleation and growth apply beyond supersaturation and solubility effects. We also provide examples of the pitfalls which can be encountered in continuous antisolvent crystallizer design when solvent effects on kinetics are not considered. Finally, we present strategies to streamline future kinetic parameter estimations and continuous crystallization process designs through reducing experimental load and raw material use. These concepts are demonstrated through a case study using a proprietary compound produced by Novartis International AG in a solvent−antisolvent system.

MATERIALS, EXPERIMENTAL METHODS, AND MODELING

In this section, we present the materials and experimental methods used for the single-stage MSMPR experiments involving combined cooling and antisolvent crystallization. We also present the steady-state MSMPR modeling process used to regress the growth and nucleation coefficients from single-stage, steady-state MSMPR experiments.

Materials. A Novartis-supplied, confidential compound served as the API for this work. Currently, the compound is produced commercially through a batch crystallization process and has already obtained U.S. Food and Drug Administration (FDA) approval. Though currently manufactured using combined cooling and antisolvent batch crystallization, the crystallization process for this drug is marked by heavy fouling, encrustation, and additional challenges due to slow crystal growth. The compound exists in a single known polymorphic state and was supplied with a purity of >99.95%. Throughout the paper, this compound will be called API. Ethanol (EtOH; KOPTEC 200 proof pure, anhydrous, CAS #64-17-5) and tetrahydrofuran (THF; Sigma-Aldrich anhydrous, >99.9%, inhibitor-free, CAS #109-99-9), the primary solvents for the system, were always used in a 92 vol % EtOH/8 vol % THF ratio. Deionized water was the antisolvent in this study.

Solubility Measurements. The solubility of API was measured at various temperatures and solvent compositions (for a total of 56 solvent composition/temperature pairs) using an Avantium Crystal16 coupled with high performance liquid chromatography (HPLC) analysis. Solubility was measured at increments of 5 °C between temperatures of 5 and 35 °C as well as solvent volume fractions of 45, 50, 55, 60, 70, 75, 80, and 90 vol % (EtOH + THF) solvent, as calculated on an API-free basis. In this paper, all volume fractions are defined based on the volumes of solvent used to create the solution: (volume of THF + volume of EtOH)/(volume of THF + volume of EtOH + volume of water). The detailed solubility measurement procedure may be seen in Supporting Information.

Single-Stage MSMPR Operation. Before continuous operation, the reactor was charged with solvent and antisolvent representing the desired steady-state solvent/antisolvent composition. API solids equivalent to the solubility of API plus an additional 1.5 g of API were added to solution to ensure that excess solids were present in solution at the start of continuous operation. This resulting solution was held overnight at the desired temperature of operation to enable equilibrium to be obtained in the crystallizer.

Continuous crystallization experiments were conducted using a single-stage MSMPR crystallizer with two continuous feeds and an intermittently withdrawn product outlet.[24] The MSMPR vessel was a 100 mL, temperature-controlled glass reactor in the Mettler-Toledo EasyMax 102 system. For all experiments, the working volume of the crystallizer was approximately 80 mL. Crystallizer contents were agitated at 350 rpm using overhead stirring. Solvent feed containing EtOH, THF, and dissolved API was continuously supplied to the MSMPR at an inlet temperature of 55 °C. Deionized water, the antisolvent, was continuously fed to the MSMPR at room temperature. To eliminate plugging, crystallizer feed lines were flushed for 5−10 s every 45−60 min during continuous operation. Crystallization product withdrawals occurred for 30 s at regular intervals of 1/10th the crystallizer residence time. A schematic of the single-stage MSMPR setup is provided in Figure 1. Further experimental details are provided in Supporting Information.

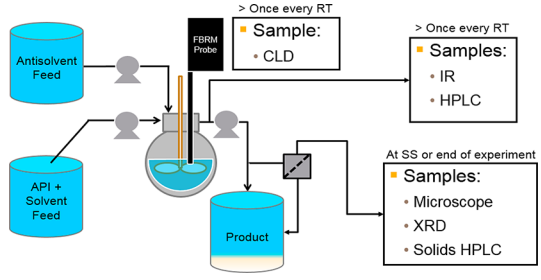

Figure 1. Single-stage MSMPR setup for kinetic parameter estimation experiments.

Continuous operation was defined to begin when both feed pumps and the product pump were started. From the start of continuous operation, the following types of samples were collected at regular intervals of at least three times per residence time: filtered HPLC samples for monitoring API concentration in the mother liquor, filtered infrared spectroscopy (IR) samples for monitoring solvent composition in the reactor, and FBRM samples for capturing the chord length distributions of crystals in the reactor. While FBRM samples were collected online, HPLC and IR analysis occurred offline. Details regarding HPLC, IR, and FBRM analysis are addressed in Supporting Information.

DOI: 10.1021/acs.cgd.7b01528
Cryst. Growth Des. 2018, 18, 1560−1570

During continuous operation, the system was allowed to transiently evolve to steady-state operation. As HPLC and IR samples were analyzed offline, steady-state operation could not be confirmed using HPLC, IR, and FBRM techniques simultaneously. Instead, we assumed the system was operating at steady state when the number of chord counts recorded by FBRM did not change by more than 5−7% and the number of particles in each chord length bin did not change appreciably for chord length distributions (CLDs) collected over two or more consecutive residence times. Sustained operation at steady-state was confirmed postexperiment using HPLC and IR data. For each steady-state experiment, steady-state operation was maintained for at least two residence times.

In some continuous crystallization experiments, multiple steady states were explored by changing operating conditions within the crystallizer. Transitions between steady states only occurred after an initial steady state was realized for greater than two residence times, and the evolution to each new steady state was monitored through continued FBRM, IR, and HPLC sampling. Each successive steady state was maintained for a minimum of two residence times using the same steady-state criteria described above.

Experimental Conditions for Steady-State MSMPR Experiments. As will be discussed in the section steady-state parameter estimation, when steady-state data are used for kinetic characterization, a minimum of six steady-state experiments are required to estimate the effect of temperature and solvent composition on growth and nucleation kinetics for an API−solvent−antisolvent system in an MSMPR crystallizer. Table 1 summarizes the experimental conditions for six continuous, single-stage MSMPR experiments which were conducted to regress the kinetics and one additional run used to validate the model.

Steady-State Population Balance Modeling. Four equations are required to formulate a steady-state MSMPR kinetic model: a material balance, a population balance, a kinetic expression for crystal nucleation, and a kinetic expression for crystal growth. At steady state, the mass balance for the liquid-phase API concentration and the size distribution of crystals in the solution can be described by following set of equations:[10]

$$C_{in} - C - \rho k_v \int n(L) L^3 \, dL = 0 \tag{1a}$$

$$\tau G \frac{dn}{dL} + n = 0 \tag{1b}$$

$$n(L = L_o) = \frac{B}{G} \tag{1c}$$

where C_{in} is the API concentration in the feed, C is the steady state API concentration in solution, and $n(L)$ is the number-based size distribution of crystals in solution, with the growth rate given by G and the nucleation rate given by B. The following assumptions are also embedded in this steady-state MSMPR model: the feed to crystallizer is free of crystals, the solution in crystallizer is well-mixed, there is negligible agglomeration and breakage among the crystals, and there is no growth dispersion.[10]

The above population balance model (eqs 1b and 1c) assumes size-independent, one-dimensional growth of crystals. By assuming L_o to be negligibly small, these equations can be further simplified to

$$n = \frac{B}{G} \exp\left(-\frac{L}{\tau G}\right) \tag{1d}$$

The growth and nucleation rates are assumed to follow power law kinetics:[25,26]

$$B = k_b \sigma^b \mu_2 \tag{1e}$$

$$G = k_g \sigma^g \tag{1f}$$

where k_b and k_g are parameters which are functions of both temperature and solvent composition, g and b are solvent composition-dependent parameters, and σ is the steady-state supersaturation defined as[25]

$$\sigma = \ln\left(\frac{C}{C_{sol}}\right) \tag{1g}$$

The second moment is used to estimate the secondary nucleation rate of API, as it captures the surface area of particles available in the crystallizer to serve as nucleation sites.[26] We also assume that secondary nucleation is the dominant nucleation mechanism in the continuous MSMPR crystallizer as at steady state, there will always be some crystals present in the solution.

Steady-State Parameter Estimation. In this work, only the growth and nucleation kinetic coefficients (k_g and k_b) are estimated. The corresponding supersaturation powers (g and b) will be fixed at their nominal values of $g = 1$ and $b = 2$; these estimates are reasonable assumptions for antisolvent systems where supersaturation levels are high.[25] The reason for fixing supersaturation powers is that, in steady-state estimation, the supersaturation and corresponding size distribution at steady-state are used to estimate the parameters. In practice, this steady-state supersaturation value cannot be known a priori and may have a value close to 1, rendering accurate estimation of g and b impossible, as these parameters will become unidentifiable under such conditions. This was the case with some of the experiments we performed. It is known that g and b do not depend on temperature, but it is possible that they depend on solvent composition.[12,25] Fixing these parameters may not accurately represent reality, but any dependency these parameters might have with respect to solvent composition will be manifested through changes in the growth and nucleation kinetic rates.

This restriction can always be removed if more experiments are completed to break the correlation between the four kinetic parameters k_g, k_b, g, and b at supersaturations substantially away from 1, while ensuring identifiability of all four parameters. However, the goal in this series of experiments is to elucidate the general trend of changes in kinetic parameters with respect to solvent composition using the minimum number of experiments and minimal material, so the strategy of fixing g and b works acceptably. This restriction on g and b can also be removed if one is using dynamic data, in which case different supersaturation values while the process is transient can provide enough excitation to estimate g and b values. We plan to explore dynamic modeling to simultaneously regress all four kinetic parameters as a function of solvent composition and temperature in a future publication.

With the above considerations, a minimum of two experiments per solvent composition are needed to identify kinetic coefficients k_g and k_b as a function of temperature at each solvent composition. To establish a

Table 1. Experimental Conditions for Single-Stage MSMPR Kinetic Experiments

						steady-state average	
run	MSMPR exp. #	temperature (°C)	solvent flow rate (mL/min)	antisolvent flow rate (mL/min)	residence time (min)	solvent volume fraction (unitless)	feed concentration (g API/kg solution)
1	1	10	0.48	0.40	90	0.44	17.431
	2	20	0.48	0.40	90	0.44	17.431
2	3	10	0.39	0.13	180	0.66	27.183
	4	30	0.39	0.13	180	0.66	27.183
3	5	10	0.64	0.40	90	0.48	19.220
	6	30	0.64	0.40	90	0.48	19.220
4	7	20	0.56	0.40	90	0.47	20.154

DOI: 10.1021/acs.cgd.7b01528
Cryst. Growth Des. 2018, 18, 1560−1570

nonlinear trend in these parameters with respect to solvent composition, a minimum of three solvent compositions should be considered. Therefore, we used a total of six experiments (Experiments 1−6 in Table 1) as a basis for the steady-state kinetic parameter regression.

The model described by equations (1a, 1d−1g) is nonlinear with respect to parameters, so estimating these parameters becomes a nonlinear optimization problem which was solved using nonlinear program (NLP) solver *fmincon* in MATLAB. To simplify the calculations and reduce errors due to numerical approximation of the integral over the size distribution, the model equations (1a and 1d) were condensed using the method of moments. The optimization problem and the set of equations to be solved within the optimization loop are as follows:

$$\min_{k_g,k_b} w_1(C - C_{exp})^2 + w_2 \sum (\mathrm{Vol}_{CSD} - \mathrm{Vol}_{CSD_{exp}})^2$$

$$\text{s.t.}$$

$$C_{in} - C - \rho k_v 3G^3 B\tau^4 = 0$$

$$\mu_3 - 3G^3 B\tau^4 = 0$$

$$G = k_g\sigma^g$$

$$B = k_b\sigma^b\left(\frac{\mu_3}{3G\tau}\right)$$

$$\sigma = \ln\left(\frac{C}{C_{sol}}\right)$$

$$g = 1$$

$$b = 2 \qquad \text{(P1)}$$

Weightings in the optimization problem were selected to normalize the values of the concentration and the volume-weighted CSDs. To complete the first portion of the regression, mother liquor API concentration data (C_{exp}) is compared with the API concentration expected in the crystallizer (C), as calculated using the MSMPR model equations. To estimate the API concentration in the MSMPR, the inlet API concentration (C_{in}), adjusted for dilution with antisolvent, is required, along with the solubility of the API at the MSMPR operating conditions (C_{sol}). To complete the second portion of the regression, the measured volume-weighted crystal size distribution (CSD), Vol_{CSD}, was approximated by the L^4-weighted chord length distribution (CLD) from the FBRM ($\mathrm{Vol}_{CSD_{exp}}$). The discussion of this weighting selection is provided in Supporting Information for interested readers. A similar conclusion was also made in one of the previous studies where the authors showed that a linear relationship exists between the fourth moments of CLD and the third moment of PSD which is in agreement with the standard industrial practice of "length weighting".[23]

RESULTS AND DISCUSSION

In this section, we present the steady-state MSMPR modeling and parameter estimation results along with the experimental results from six experiments, the minimum number of experiments required to establish simultaneous dependence of growth and nucleation kinetics on solvent composition and temperature. Experimentally determined solubility data are also presented for API.

Solubility Measurement and Modeling Results. The solubility curves of API in mixtures of ethanol, THF, and water are presented in Figure 2. Though a strong function of temperature, API solubility is an even stronger function of solvent composition. As the fraction of antisolvent in solution increases, the solubility of API monotonically decreases at all temperatures studied. Minimally, both temperature and solvent composition must be included in calculations of solubility and supersaturation for the MSMPR model.

To model both the solvent composition and temperature dependence of solubility, a two-step approach was used. First, we modeled the solubility as a function of temperature using the Apelblat equation for each solvent composition as follows:[27]

$$\ln(S_i) = \beta_{1i} + \frac{\beta_{2i}}{T} + \beta_{3i}\ln(T) \qquad \text{(4a)}$$

Table 2. Experimental Results for Single-Stage MSMPR Kinetic Experiments

		steady-state average			
run	MSMPR exp. #	solvent volume fraction (unitless)	supersaturation (unitless)	concentration (g API/kg solution)	yield (mass %)
1	1	0.44	1.19	1.17	93.29
	2	0.44	1.05	1.34	92.31
2	3	0.66	1.26	10.24	62.34
	4	0.66	1.05	15.11	44.40
3	5	0.48	1.75	2.92	84.80
	6	0.48	1.27	3.23	83.19
4	7	0.47	1.32	2.29	88.64

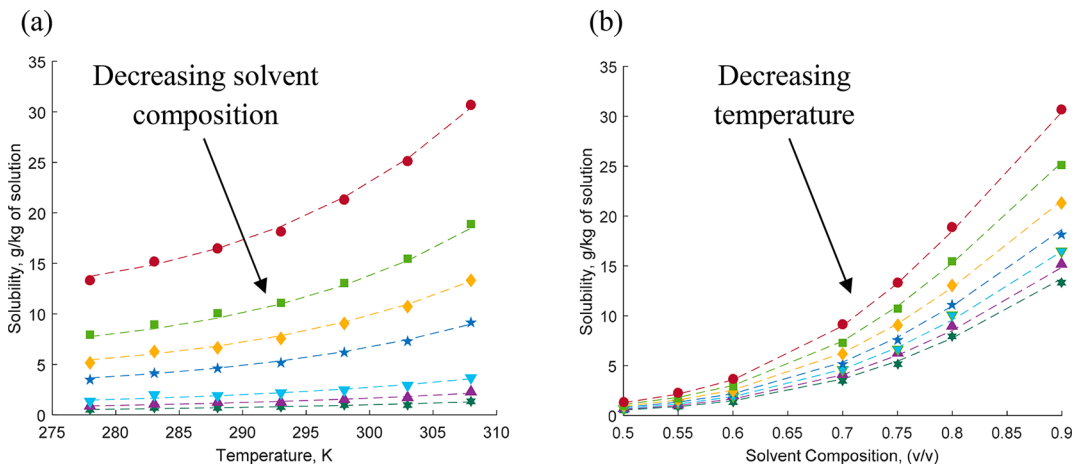

Figure 2. Regressed two-parameter Apelblat solubility model with solubility data. API solubility, measured at solvent volume fractions of 50, 55, 60, 70, 75, 80, and 90 vol % (EtOH + THF) solvent, is a strong function of solvent composition (a) but a weaker function of temperature (b), as measured at increments of 5 °C between temperatures of 5 and 35 °C.

DOI: 10.1021/acs.cgd.7b01528
Cryst. Growth Des. 2018, 18, 1560−1570

where S_i is the solubility at ith solvent composition and β_{1i}, β_{2i}, and β_{3i} are the corresponding model parameters.

In the second step, each of the parameters β_1, β_2, and β_3 were expanded as a function of solvent composition using the following model

$$\beta_k = \alpha_{k1} + \alpha_{k2} x_s + \frac{\alpha_{k3}}{x_s} + \alpha_{k4} \ln(x_s) \tag{4b}$$

The rationale for the above model structure is that the Apelblat equation was found to also model solubility well as a function of solvent composition. Combining the two models above gives us one unified model for solubility as a function of both temperature and solvent composition as follows:

$$\ln(S_i) = \left(\alpha_{11} + \alpha_{12} x_s + \frac{\alpha_{13}}{x_s} + \alpha_{14} \ln(x_s)\right) + \frac{\alpha_{21} + \alpha_{22} x_s + \frac{\alpha_{23}}{x_s} + \alpha_{24} \ln(x_s)}{T} + \left(\alpha_{31} + \alpha_{32} x_s + \frac{\alpha_{33}}{x_s} + \alpha_{34} \ln(x_s)\right) \ln(T) \tag{4c}$$

The solubility data collected below x_s = 50 vol % are very noisy, and therefore only the data between x_s = 50 vol % − 90 vol % and T = 5 °C − 35 °C were used to calibrate the above model. At solvent fractions of x_s < 50 vol %, the solubility curve is relatively

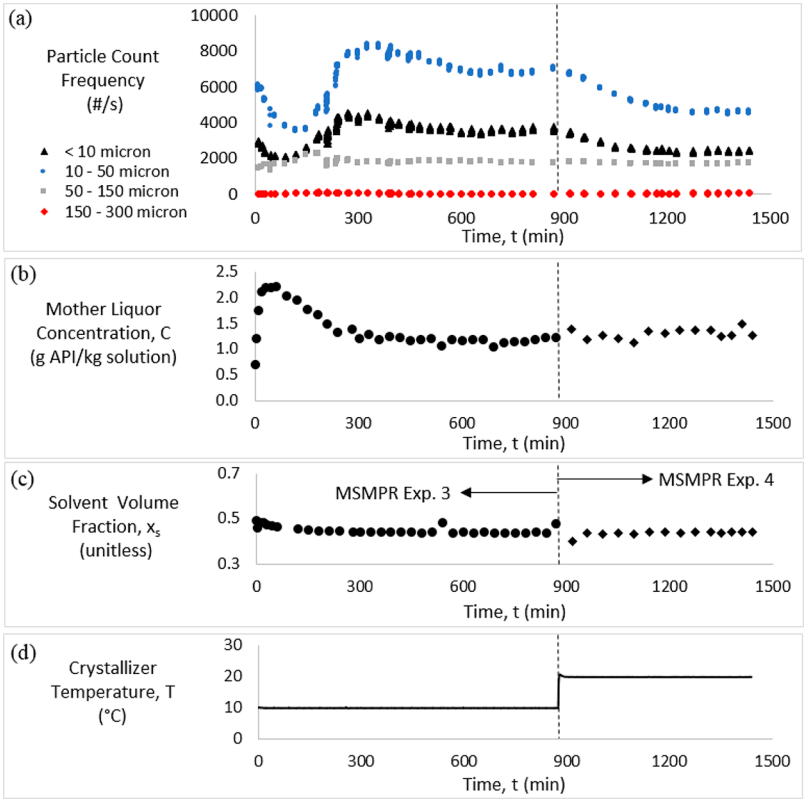

Figure 3. Run 2 experimental results for continuous API crystallization. Two steady-states, in MSMPR experiments 1 and 2, were achieved sequentially with respect to (a) FBRM particle counts, (b) API concentration in the mother liquor, (c) solvent volume fraction, and (d) crystallizer temperature.

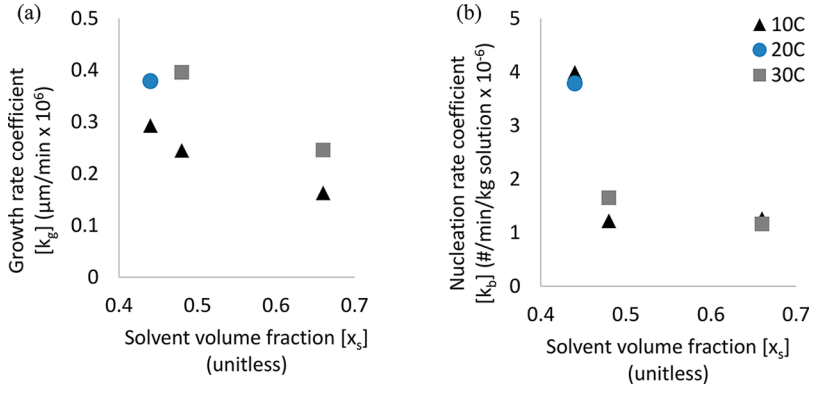

Figure 4. Regressed kinetic coefficients for (a) growth as a function of solvent composition and temperature, and (b) nucleation as a function of solvent composition, as k_b is a weak function of temperature.

DOI: 10.1021/acs.cgd.7b01528
Cryst. Growth Des. 2018, 18, 1560−1570

flat, and measured changes in the solubility on the order of the error in the experimental solubility measurements. The predicted solubility is displayed along with the experimentally measured solubility in Figure 2; the calibrated model represents the experimental data very well.

MSMPR Crystallization of API. During a single continuous run, multiple steady states were approached to collect experimental data for kinetic parameter regression. Results for these experiments are tabulated in Table 2. For example, during Run 2, two different steady-states were maintained sequentially in MSMPR experiments 1 and 2 (Figure 3). Initially, the MSMPR crystallizer operated at a temperature of 10 °C with a solvent fraction of 0.44 and a residence time of 90 min. The system achieved steady-state operation in approximately seven residence times and maintained steady-state before a step change in temperature from 10 to 20 °C induced the system to transition to a second, different steady state. Approximately four residence times later, the crystallizer reached the second steady-state. In each case, steady-state operation was assessed online using FBRM (Figure 3a) and confirmed offline using HPLC data (Figure 3b) and IR data (Figure 3c).

Kinetic Parameter Estimates at Steady State. Kinetic parameter coefficients for nucleation and growth were regressed using the procedure outlined in Section 2.4. Results are provided in Figure 4.

There is a significant effect of solvent composition on both growth and nucleation kinetics. As shown through these six

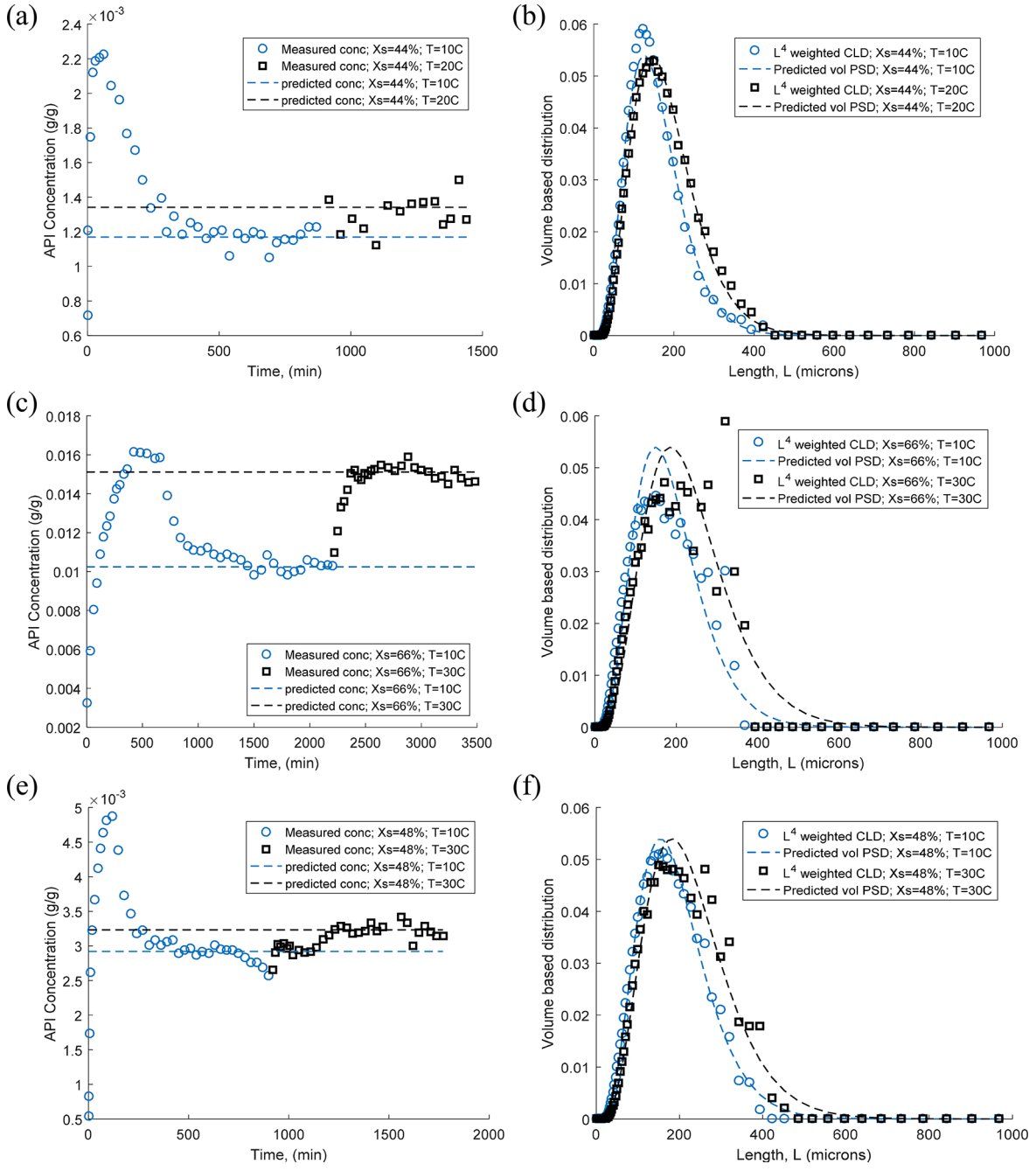

Figure 5. Comparison of experimental data with predicted crystallizer performance using regressed kinetic parameters at each solvent composition and temperature pair. Steady-state concentration is predicted for MSMPR experiments 1 and 2 (a); 3 and 4 (c); and 5 and 6 (e). CSDs are also predicted for MSMPR experiments 1 and 2 (b); 3 and 4 (d); and 5 and 6 (f).

DOI: 10.1021/acs.cgd.7b01528
Cryst. Growth Des. 2018, 18, 1560−1570

experiments, both growth and nucleation kinetic parameters tend to increase as the solvent volume fraction decreases, or as the antisolvent volume fraction increases. Even over a modest change in solvent fraction of approximately 22 vol %, the kinetic growth coefficient almost triples. Similarly, over a modest change in solvent fraction of approximately 4 vol % from 48 vol % to 44 vol % solvent, the kinetic nucleation coefficient triples. For the range of solvent compositions studied in the API system, it appears that the crystal growth coefficient changes gradually as a function of solvent composition, while crystal nucleation kinetics demonstrate almost exponential changes as functions of solvent composition. Further investigation is required to generalize these results to other API−solvent−antisolvent systems as well as elucidate why, on a molecular level, solvent composition has such drastic effects on crystal nucleation and growth, beyond the influences of solubility and supersaturation.

The corresponding fits of different experimental data sets are shown in Figure 5. Each pair of figures represents experimental data for two different steady states at a single solvent composition.

For each pair of steady states, corresponding to data collected at a single solvent composition, there is acceptable agreement between the experimental data and the values predicted using the regressed kinetic parameters. This agreement applies to both the mother liquor concentration data as well as the CLD data. At 10 °C and adjusted for feed concentration effects, mother liquor API concentration was substantially higher at steady-state operation in MSMPR Experiment 3 versus MSMPR Experiment 1, even though the residence time was twice as long. This indicates the depletion of supersaturation occurs more rapidly at lower solvent fractions, qualitatively indicating enhanced kinetic rates at increased antisolvent fractions. Considerations of the CSDs at the same temperatures indicate the same trends, giving additional credence to the trends realized in the regressed nucleation and growth kinetic coefficients.

With respect to temperature, it is observed that growth rate coefficients change significantly with temperature across all the solvent compositions. However, the change in nucleation rate coefficients does not appear to be significant, and for further analysis of this system, the nucleation coefficient is assumed to be constant with respect to temperature for all solvent compositions. For three solvent compositions studied, the nucleation coefficients are assumed to be the average of estimated values:

$$k_{b_{44\%}}\left[\frac{\#}{\text{min·kg solution}}\right] = 3.89205 \times 10^{6} \tag{5a}$$

$$k_{b_{48\%}}\left[\frac{\#}{\text{min·kg solution}}\right] = 1.4394 \times 10^{6} \tag{5b}$$

$$k_{b_{66\%}}\left[\frac{\#}{\text{min·kg solution}}\right] = 1.2147 \times 10^{6} \tag{5c}$$

For growth rate coefficients, Arrhenius expression is used to fit the temperature dependency, and for three solvent compositions studied, the expressions are as follows:

$$k_{g_{44\%}}\left[\frac{m}{\text{min}}\right] = 0.000536\ \exp^{(-2125.5/T)} \tag{6a}$$

$$k_{g_{48\%}}\left[\frac{m}{\text{min}}\right] = 0.000351\ \exp^{(-2056/T)} \tag{6b}$$

$$k_{g_{66\%}}\left[\frac{m}{\text{min}}\right] = 0.00008199\ \exp^{(-1760/T)} \tag{6c}$$

As antisolvent fraction increases, potential for the API to transition from the liquid phase to the crystalline phase increases and is reflected in the decreasing activation energy associated with growth. Figure 6 summarizes the revised growth rate and nucleation rate coefficients as a function of temperature and solvent composition.

To check the validity of constant nucleation coefficient assumption, the experimental data set for MSMPR experiments 1−6 is refitted with the average, temperature-independent nucleation rate coefficient; fits are shown in Figure 7. It is clear from these plots that the model predictions are still in good agreement with the data, especially the steady state concentration fits.

Solvent-Dependent Parameter Model Validation. Finally, the model was finally validated using steady-state data from MSMPR Experiment 7 obtained at solvent composition $x_s = 47\%$, residence time, $\tau = 90$ min, and temperature $T = 20$ °C. This data set is quite distinct from all the data sets used in the model calibration step and is ideal to check the interpolation of estimated growth and nucleation rate coefficients. Temperature dependency is calculated using the Arrhenius relation, whereas solvent composition dependency is calculated using linear interpolation between the two adjacent solvent compositions. The corresponding kinetic parameters used to validate this data set are $k_g = 0.3304 \times 10^{-6}\left[\frac{m}{\text{min}}\right]$ and $k_b = 2.0526 \times 10^{6}\left[\frac{\#}{\text{min}}\right]$. The results of validation are summarized in Figure 8, where it is clear that the model predicts both steady state CSD and API concentration with reasonable accuracy. It is notable that the

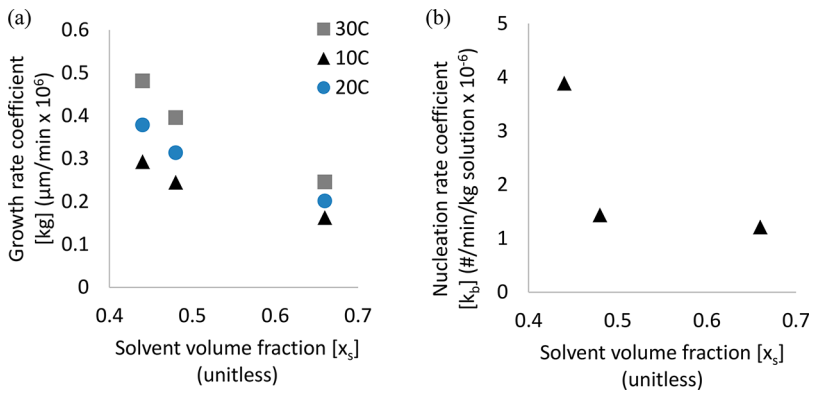

Figure 6. Regressed kinetic coefficients for (a) growth as a function of solvent composition and Arrhenius-dependence on temperature, and (b) nucleation as an averaged function of solvent composition but not temperature.

DOI: 10.1021/acs.cgd.7b01528
Cryst. Growth Des. 2018, 18, 1560−1570

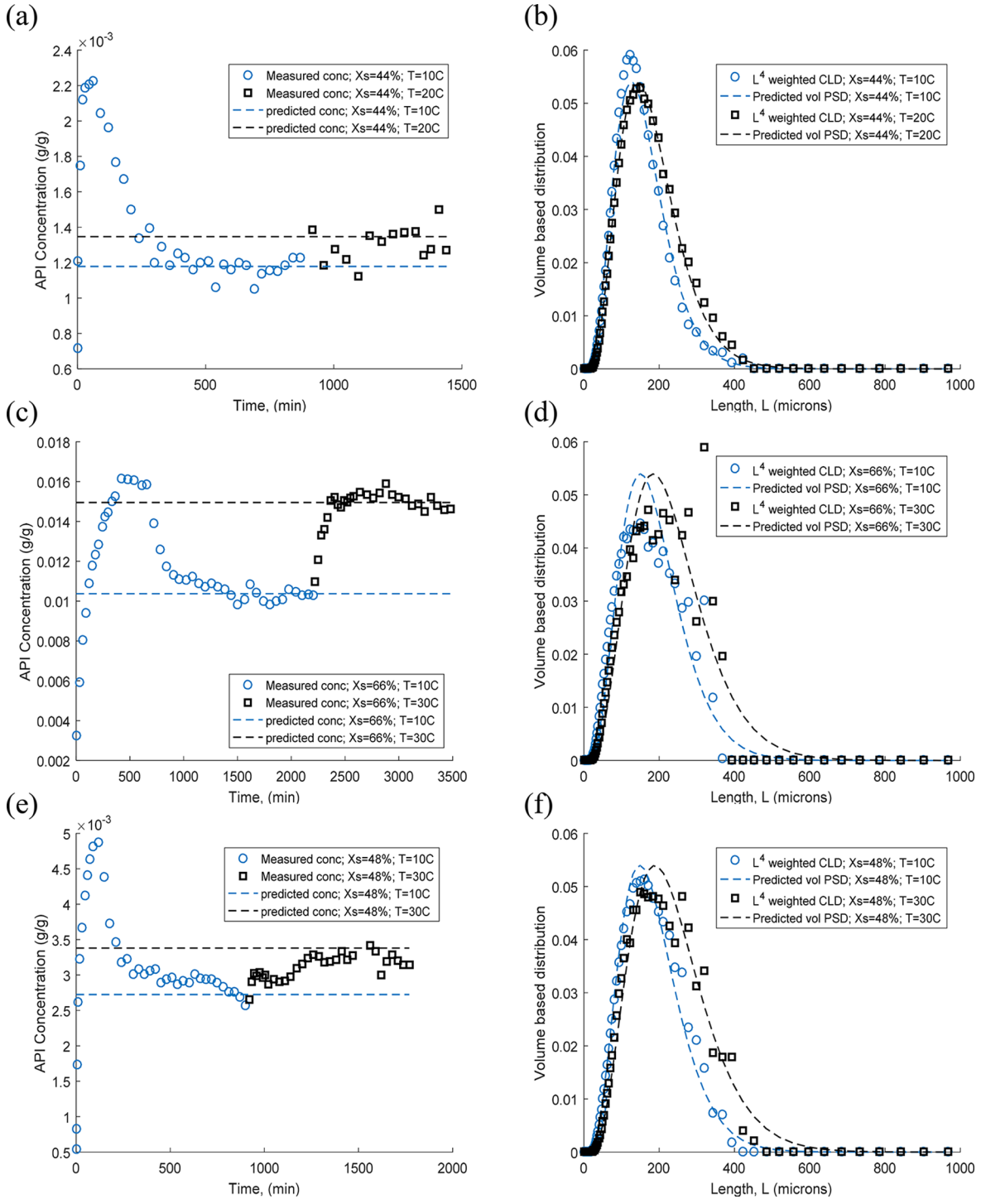

Figure 7. Comparison of experimental data with predicted crystallizer performance using regressed kinetic parameters at each solvent composition and temperature pair, assuming temperature-independent nucleation parameters. Steady-state concentration is predicted for MSMPR experiments 1 and 2 (a); 3 and 4 (c); and 5 and 6 (e). CSDs are also predicted for MSMPR experiments 1 and 2 (b); 3 and 4 (d); and 5 and 6 (f).

growth and nucleation parameters, as well as the solubility, are so sensitive to solvent composition that even a 1 vol % change in solvent composition can manifest substantially lower steady-state API concentrations in the mother liquor, resulting in higher yields. For example, Experiment 7 exhibited a yield of approximately 88.6% at x_s = 47 vol % and T = 20 °C compared to Experiments 5, in which yields of 84.8% were exhibited at lower temperature T = 10 °C. Similarly, average yield was only 83.2% in Experiment 6 at a steady-state of x_s = 48 vol % and T = 30 °C. Therefore, temperature is not driving the yield increases. Instead, solvent composition is driving the yield increases, and very slight changes in solvent composition can drastically change the growth and nucleation rates, unlocking lower steady-state mother liquor concentrations and, ultimately, higher yields.

Prediction of Crystallizer Performance at Different Solvent Compositions. As mentioned in the Introduction, the effect of solvent composition on growth and nucleation kinetics is often ignored in studies, which was the key motivation behind

DOI: 10.1021/acs.cgd.7b01528
Cryst. Growth Des. 2018, 18, 1560−1570

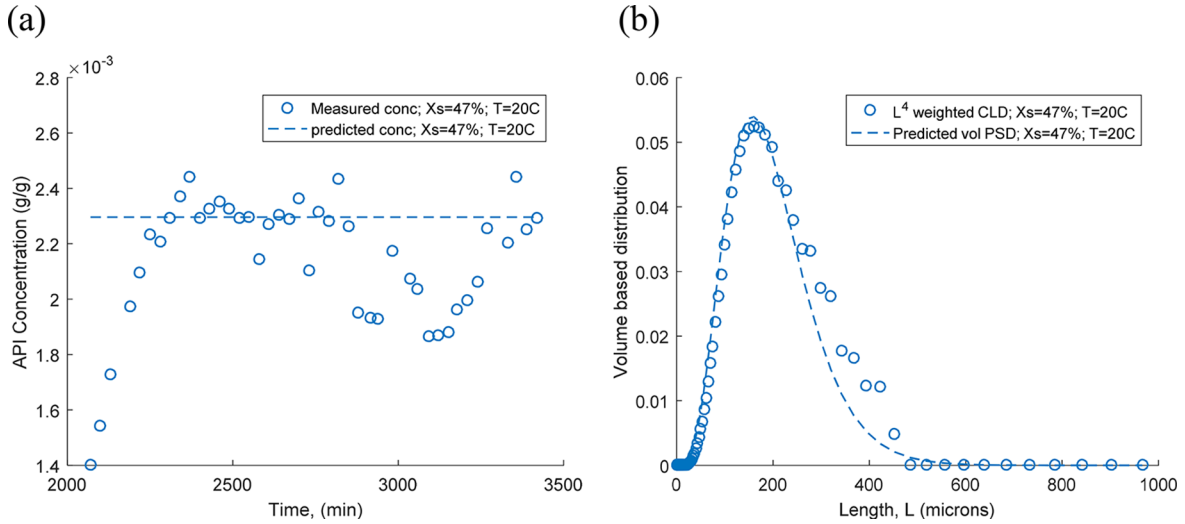

Figure 8. Validation of solvent-dependent kinetic parameter model, assuming temperature-independent nucleation parameters. Steady-state concentration (a) and CSD (b) are acceptably predicted for MSMPR experiment 7. At approximately t = 2700 min, the API/solvent feed line partially fouled, which caused the API mother liquor concentration to decrease in the crystallizer. Once the feed lines were cleared, the API mother liquor concentration recovered and approached the steady-state value again.

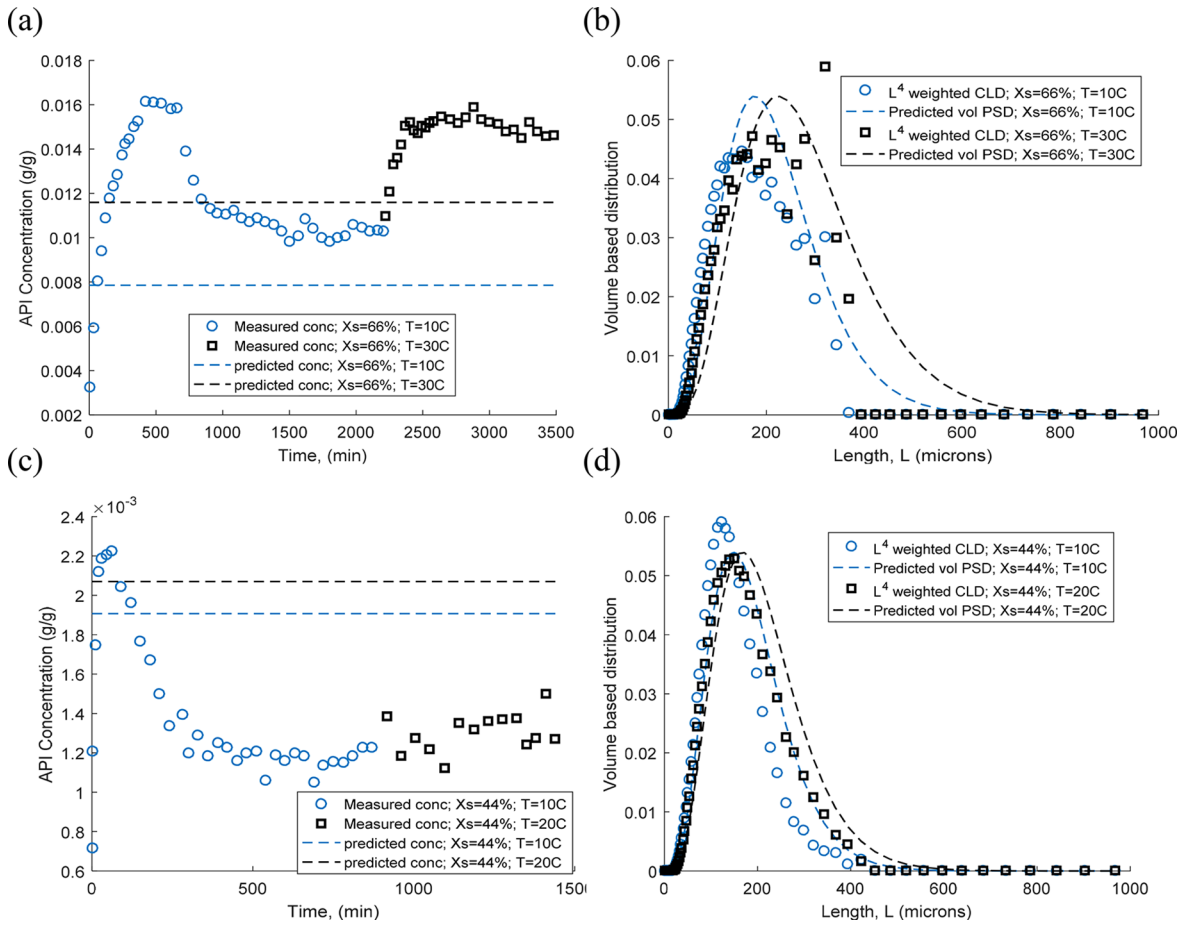

Figure 9. Comparison of experimental data with predicted crystallizer performance using kinetic parameters regressed at x_s = 48 vol % corrected for temperature using Arrhenius expression. Steady-state concentration is predicted for MSMPR experiments 3 and 4 (a); and 5 and 6 (c). CSDs are also predicted for MSMPR experiments 3 and 4 (b); and 5 and 6 (d).

this work. Now, it has been shown in this paper that solvent dependency does matter, but what happens if we ignore this? To check such a scenario, the parameters estimates at x_s = 48% will be used to predict the experimental data set at x_s = 44% and x_s = 66% . The results are summarized in Figure 9.

If kinetic dependence on solvent composition is neglected, crystallizer performance is not acceptably predicted in either case. As shown in Figure 9, neither mother liquor API concentration nor particle size distribution are acceptably predicted when attempting to estimate crystallizer performance using kinetic

DOI: 10.1021/acs.cgd.7b01528
Cryst. Growth Des. 2018, 18, 1560−1570

parameters regressed at solvent compositions that are not in the immediate vicinity of the predicted crystallizer operation. For instance at x_s = 66%, the crystal growth rate is overpredicted, resulting in CSD projections that are shifted to the right of the actual CSDs and mother liquor API estimates that are unacceptably low. As a result, yield is overpredicted (71.3% predicted versus 62.3% actual at 10 °C) and would result in selecting a suboptimal crystallization process during the process design phase. More surprisingly, using kinetic parameters for solvent compositions even in a close vicinity results in poor crystallizer performance due to the exponential behavior of the nucleation kinetic coefficient as a function of solvent composition. For example, predicting crystallizer performance at x_s = 44% results in substantial errors. Both the crystal nucleation rate and crystal growth rate are underpredicted, manifesting in an incorrect prediction of the competition between nucleation and growth to reduce supersaturation. As a result, steady-state mother liquor API concentrations are predicted to be too high, resulting in falsely low yield predictions (89.1% predicted versus 93.2% actual at 10 °C). Again, this would result in selecting a suboptimal crystallization process during the process design phase. The inability to predict crystallizer performance at solution compositions in the local vicinity as well as at drastically different solvent compositions further demonstrates the need to elucidate the functional relationship of kinetic parameters with respect to solvent composition while completing continuous antisolvent crystallization process design.

CONCLUSIONS

In this paper, we presented a methodology for determining kinetic parameter solvent dependence using a minimum number of steady-state, continuous MSMPR experiments. By assuming that g and b are constants, we can quickly regress kinetic parameter coefficients to demonstrate solvent effects on crystal nucleation and growth kinetics using a minimum of six steady-state MSMPR experiments which cover the operational range of interest and span at least three solvent compositions. We can also use experimental data near supersaturations of σ = 1, which would render g and b unidentifiable if all four kinetic parameters were to be regressed simultaneously. This method is useful for rapid kinetic screening and continuous crystallization process development, especially in cases where API availability is limited, such as in early stage research and development.

For this particular system, API in EtOH/THF/water solutions, both nucleation and growth kinetic coefficients are functions of both solvent composition and temperature. Growth and nucleation are affected to differing degrees as solvent composition changes, and we demonstrated that these effects go beyond affecting solubility and supersaturation. Kinetic parameters for a single solvent composition were shown to incorrectly predict crystallizer performance at a different solvent composition, further highlighting the fact that it is crucial to account for solvent effects on kinetic parameters when determining system kinetics for crystallizer process design. Both CSDs and API concentration in the mother liquor were erroneously predicted at steady state. As a result, both the product CSD, crystal morphology, and yield will be affected by neglecting solvent dependence. Furthermore, solvent effects may have a stronger influence than temperature effects, which is especially true at low solvent fractions in this particular system.

As rapid API crystallization kinetic characterization becomes increasingly important in early stage crystallization process development, the number of experiments required to establish a kinetic model should be minimized. We plan to explore simultaneous solvent-dependent kinetic parameter regression of all four kinetic parameters, k_g, k_b, b, and g, using transient MSMPR data for combined cooling and antisolvent crystallization systems in the future to further reduce the number of experiments required to establish a kinetic crystallization model. We also plan to continue this work as we optimize a multistage MSMPR cascade using this parameter regression method coupled with solvent- and temperature-dependent kinetic models.

ASSOCIATED CONTENT

Supporting Information

The Supporting Information is available free of charge on the ACS Publications website at DOI: 10.1021/acs.cgd.7b01528.

Detailed solubility measurement procedure, expanded procedures for MSMPR operation, liquid- and solid-phase characterization, selection of appropriate FBRM CLD weighting (PDF)

AUTHOR INFORMATION

Corresponding Author

*E-mail: myerson@mit.edu.

ORCID

Richard D. Braatz: 0000-0003-4304-3484

Allan S. Myerson: 0000-0002-7468-8093

Funding

Novartis-MIT Center for Continuous Manufacturing, National Science Foundation (Grant No. 1122374).

Notes

The authors declare no competing financial interest.

ACKNOWLEDGMENTS

We thank the Novartis-MIT Center for Continuous Manufacturing for funding and technical guidance. We also acknowledge the National Science Foundation, Grant No. 1122374, for funding. Any opinion, findings, and conclusions or recommendations expressed in this material are those of the authors and do not necessarily reflect the views of the National Science Foundation.

ABBREVIATIONS

API, active pharmaceutical ingredient; acronym for confidential compound
CLD, chord length distribution
CSD, crystal size distribution
EtOH, ethanol
FBRM, focused beam reflectance measurement
FDA, Food and Drug Administration
HPLC, high performance liquid chromatography
IR, infrared spectroscopy
MSMPR, mixed-suspension, mixed-product removal
NLP, nonlinear program
THF, tetrahydrofuran
PXRD, powder X-ray diffraction

Variable Definitions

B, nucleation rate
b, nucleation rate power
C, API concentration in crystallizer mother liquor
C_{exp}, experimental API concentration in mother liquor
C_{in}, inlet API concentration, adjusted for antisolvent addition
C_{sol}, API solubility concentration
G, growth rate

DOI: 10.1021/acs.cgd.7b01528
Cryst. Growth Des. 2018, 18, 1560−1570

g, growth rate power
k_b, nucleation rate coefficient
k_g, growth rate coefficient
k_v, volume shape factor
L, crystal characteristic length
L_0, size-zero nuclei length
n, population density
n_{in}, population density of particles at crystallizer inlet
S_i, API solubility concentration
T, temperature
v, solvent volume
Vol_{CSD}, predicted volume-based CSD
$Vol_{CSD,exp}$, experimental volume-based CSD
w_i, ith weighting factor
x_s, solvent volume fraction, defined as $\frac{v_{THF} + v_{EtOH}}{v_{THF} + v_{EtOH} + v_{H_2O}}$
α_{kl}, lth Apelblat parameter at kth solvent composition
β_{ji}, jth Apelblat parameter at ith solvent composition
μ_i, ith moment of the size distribution
ρ, particle density
σ, supersaturation
τ, residence time

REFERENCES

(1) Variankaval, N.; Cote, A. S.; Doherty, M. F. *AIChE J.* **2008**, *54* (7), 1682−1688.
(2) Giulietti, M.; Seckler, M.; Derenzo, S.; Ré, M.; Cekinski, E. *Braz. J. Chem. Eng.* **2001**, *18* (4), 423−440.
(3) Tung, H.-H. *Crystallization of Organic Compounds: An Industrial Perspective*; Wiley: Hoboken, NJ, 2009.
(4) Plumb, K. *Chem. Eng. Res. Des.* **2005**, *83* (6), 730−738.
(5) Alvarez, A. J.; Myerson, A. S. *Cryst. Growth Des.* **2010**, *10* (5), 2219−2228.
(6) Cervera-Padrell, A. E.; Skovby, T.; Kiil, S.; Gani, R.; Gernaey, K. V. *Eur. J. Pharm. Biopharm.* **2012**, *82* (2), 437−456.
(7) Vervaet, C.; Remon, J. P. *Chem. Eng. Sci.* **2005**, *60* (14), 3949−3957.
(8) Lindenberg, C. *Optimizing the Precipitation of Organic Compounds*; Swiss Federal Institute of Technology: Zürich, 2009.
(9) Nagy, Z. K.; Aamir, E. *Chem. Eng. Sci.* **2012**, *84*, 656−670.
(10) Randolph, A. D.; Larson, M. A. *Theory of Particulate Processes: Analysis and Techniques of Continuous Crystallization*; Academic Press: London, 1971.
(11) Ramkrishna, D.; Singh, M. R. *Annu. Rev. Chem. Biomol. Eng.* **2014**, *5* (1), 123−146.
(12) Genck, W. J. *Temperature Effects on Growth and Nucleation Rates in Mixed Suspension Crystallization*, 1969 *Retrospective Theses and Dissertations*. 4105, http://lib.dr.iastate.edu/rtd/4105.
(13) Woo, X. Y.; Tan, R. B. H.; Chow, P. S.; Braatz, R. D. *Cryst. Growth Des.* **2006**, *6* (6), 1291−1303.
(14) Ridder, B. J.; Majumder, A.; Nagy, Z. K. *Ind. Eng. Chem. Res.* **2014**, *53* (11), 4387−4397.
(15) Granberg, R. a.; Ducreux, C.; Gracin, S.; Rasmuson, Å. C. *Chem. Eng. Sci.* **2001**, *56* (7), 2305−2313.
(16) Kubota, N. *J. Cryst. Growth* **2008**, *310* (22), 4647−4651.
(17) Luo, Y. H.; Wu, G. G.; Sun, B. W. *J. Chem. Eng. Data* **2013**, *58* (3), 588−597.
(18) Lindenberg, C.; Krättli, M.; Cornel, J.; Mazzotti, M.; Brozio, J. *Cryst. Growth Des.* **2009**, *9* (2), 1124−1136.
(19) Tavare, N. S. *Industrial Crystallization: Process Simulation Analysis and Design*, 1st ed.; Plenum Publishing Corporation: New York, 1995.
(20) Zhao, Y.; Hou, B.; Jiang, X.; Liu, C.; Wang, J. *J. Chem. Eng. Data* **2012**, *57* (3), 952−956.
(21) Nonoyama, N.; Hanaki, K.; Yabuki, Y. *Org. Process Res. Dev.* **2006**, *10* (4), 727−732.
(22) Trifkovic, M.; Sheikhzadeh, M.; Rohani, S. *Ind. Eng. Chem. Res.* **2008**, *47* (5), 1586−1595.
(23) Kee, N. C. S.; Arendt, P. D.; Goh, L. M.; Tan, R. B. H.; Braatz, R. D. *CrystEngComm* **2011**, *13*, 1197−1209.
(24) Ferguson, S.; Morris, G.; Hao, H.; Barrett, M.; Glennon, B. *Chem. Eng. Sci.* **2013**, *104*, 44−54.
(25) Myerson, A. S. *Handbook of Industrial Crystallization*, 2nd ed.; Butterworth-Heinemann: Woburn, MA, 2002.
(26) Frawley, P. J.; Mitchell, N. A.; Clifford, T. O.; Hutton, K. W. The effects of supersaturation, temperature, agitation, and seed surface area on the secondary nucleation of paracetamol in ethanol solutions. *Chem. Eng. Sci.* **2012**, *75*, 183−197.
(27) Manzurola, E.; Apelblat, A. *J. Chem. Thermodyn.* **2002**, *34* (7), 1127−1136.

DOI: 10.1021/acs.cgd.7b01528
Cryst. Growth Des. 2018, 18, 1560−1570